High Precision X-ray Measurements 2021

Probing Electron Properties in ECR Plasmas using X-ray Bremsstrahlung and Fluorescence Emission

Università degli Studi di Catania

INFN Istituto Nazionale di Fisica Nucleare

Bharat Mishra

Dipartimento di Fisica e Astronomia "Ettore Majorana", Università degli Studi di Catania, Catania, Italy
Istituto Nazionale di Fisica Nucleare – Laboratori Nazionali del Sud, Catania, Italy

09 June 2021
Virtual Event

Brief Overview

System of interest

Electron Cyclotron Resonance (ECR) Plasmas

Routinely used as ion sources to supply highly-charged beams to accelerators

Electron heating using microwaves and confinement using magnetic trap

Energy transfer not spatially homogenous, resultant plasma anisotropic in density and energy

Why study them?

Fundamental and Applied Research

Wave-plasma coupling in ECRIS not fully exploited

Beam intensity and emittance correlated with plasma instabilities [1], non-uniform density distribution [2] and variation of magnetic field [3]

New facilities like PANDORA require precise inputs on space-resolved properties

How to study them?

Direct and Indirect Methods

Various quantities of interest can be estimated using appropriate experiments

Direct methods: Precise determination of density, EEDF, energy etc. but perturb the plasma. *Ex: Langmuir probes*

Indirect methods: No plasma perturbation, but not sensitive to the full range of energies. *Ex: Optical emission spectroscopy, ECR emission spectroscopy, X-ray spectroscopy*

Warm electron distribution : Soft X-Ray Spectroscopy

Space-resolved X-ray maps obtained with CCD + pinhole setup

Volumetric X-ray spectra obtained with SDD + collimator setup

Space-resolved electron distribution simulations + Fluorescence reaction rate + Space-resolved geometrical efficiency

\+

Theoretical emission model

\+

3D SPACE-RESOLVED ELECTRON DENSITY, EEDF AND TEMPERATURE

Confined electron density, temperature, EEDF estimate

Loss electron current density estimate

[1] O.Tarvainen, I. Izotov, D. Mansfeld, V. Skalgya, S. Golubev, T. Kalvas, H. Koivisto , J. Comppula, R. Cronholm, J. Laulainen and V. Toivanen, Plasma Sources Sci. Technol.**23,** 025020 (2014)
[2] D. Mascali, G. Torrisi, L. Neri, G. Sorbello, G. Castro, L. Celona and S. Gammino, Eur. Phys. J. D **69**, 27 (2015).
[3] L. Celona, G. Ciavola, F. Consoli, S. Gammino, F. Maimone, P. Spaedtke, K. Tinschert, R. Lang, J. Mader, J. Rosbach, S. Barbarino, R. S. Catalano and D. Mascali, Rev. Sci. Instrum. **79**, 023305 (2008).

ECRIS: Operation and Properties

Heating

Magnetic field B applied longitudinally causing electrons to gyrate at frequency $\omega_c = \frac{eB}{m_e}$

R-wave launched into the plasma at same frequency, leading to resonance heating

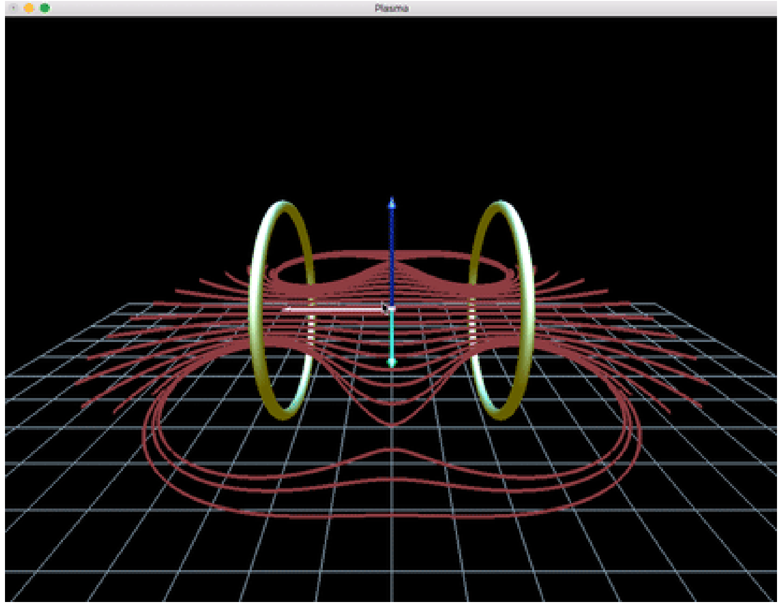

Confinement

From fluid model, adiabatic invariant defined as $\mu = \frac{1}{2}\frac{mv_\perp^2}{B} = const$

Min-B configuration to trap electrons longitudinally, prolonged heating for energetic reactions

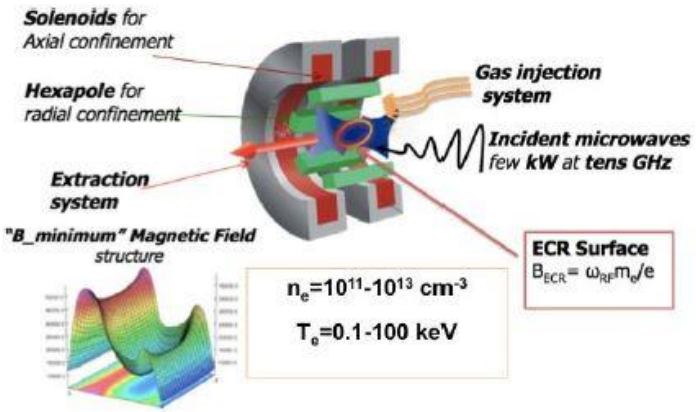

Schematic of ECRIS operation [4]

$$\omega = \omega_c = \frac{eB}{m}$$

$$P \propto E^2$$

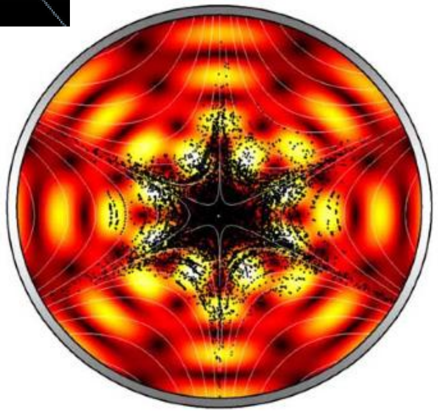

EM field in midplane at f ~14 GHz [5]

[4] D. Mascali, A. Musumarra, F. Leone, F.P. Romano, A. Galatá, S. Gammino and C. Massimi, Eur. Phys. J. A **53**, 145 (2017).
[5] S. Gammino, G. Ciavola, L. Celona, D. Mascali and F. Maimone, IEEE Transactions on Plasma Science **36**, 4 (2008)

ECRIS: Operation and Properties (contd.)

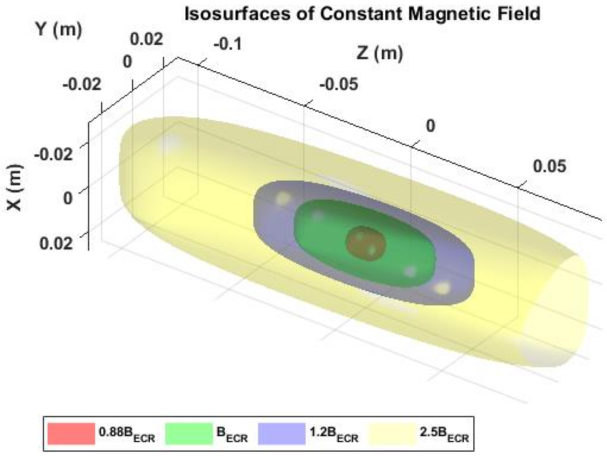

B-field surfaces in a plasma chamber with the closed ECR surface

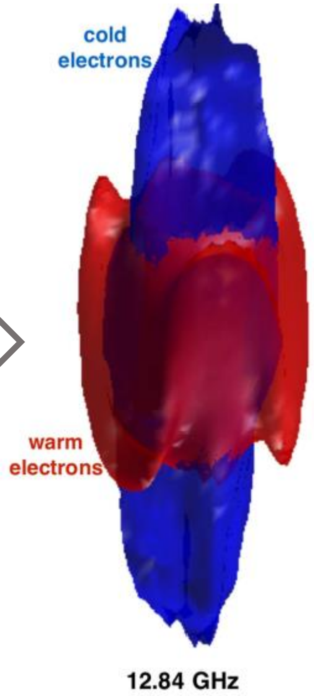

3D structure of plasma from simulations – the spatial anisotropy and non-homogeneity with respect to density and energy is visible [6]

Energetic electrons (~ keV) and radiation interact with the ions through multiple processes (ionization, excitation etc.) to produce high charge states (NLTE population kinetics solved with CR model)

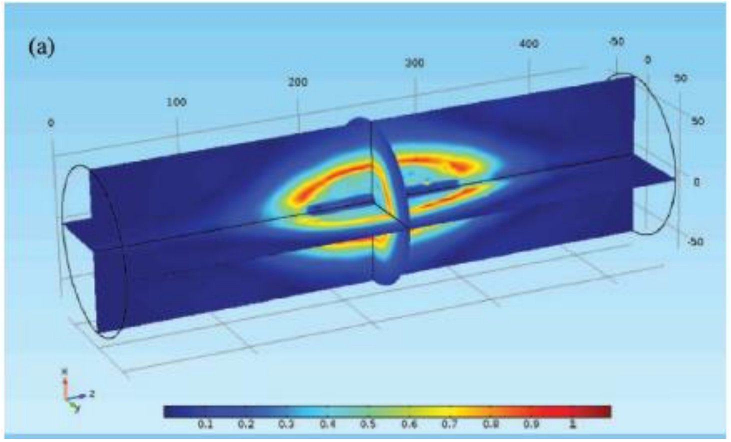

Net particle density distribution (positive charge in blue, negative in red [7]

[6] R. Racz, D. Mascali, S. Biri, C. Caliri, G. Castro, A. Galata, S. Gammino, L. Neri, J. Palinkas, F.P. Romano and G. Torrisi, Plasma Sources Sci. Technol. **26**, 075011 (2017).
[7] D. Mascali, L. Neri, L. Celona, G. Castro, G. Torrisi, S. Gammino, G. Sorbello and G. Ciavola, Rev. Sci. Instrum. **85**, 02A511 (2014)

PANDORA: Plasmas for Astrophysics, Nuclear Decays Observation and Radiation for Archaeometry
A new ECR Ion Trap for in-plasma β-decay measurements

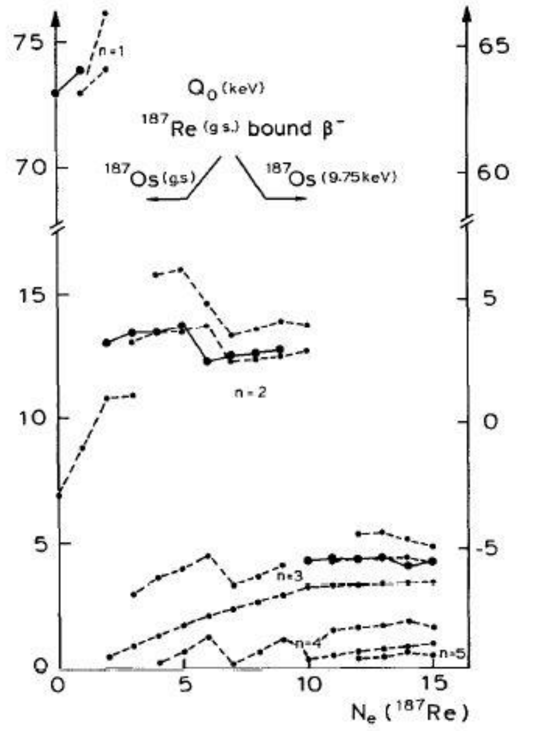

Q-value of bound state ^{187}Re→^{187}Os transitions as a function of degree of ionization [8]

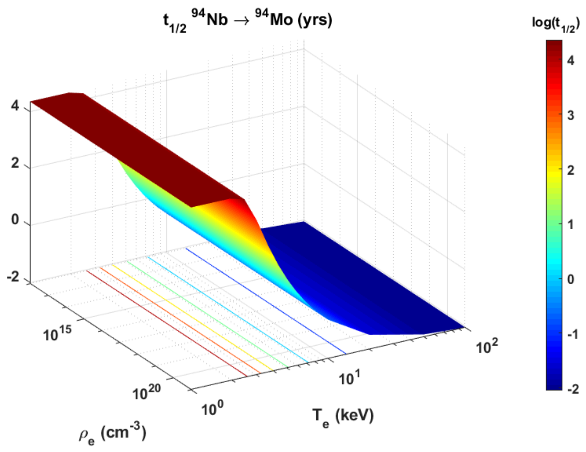

Modification of half-life as a function of plasma parameters – effect of ion CSD

$$f^*_{IF(m)} = \int_1^{E_{max}} (E^2 - 1)^{1/2} E q^2 F_0 S_{(m)} f_d \mathrm{d}E \qquad \text{(continuum decay)}$$

$$f^*_{IF(m)} = \sum_y \sigma_y(\pi/2)[g_x \text{ or } f_x]^2 q^2 S_{(m)x} \qquad \text{(bound state decays/captures)}$$

Theory of Takahashi and Yokoi [8]

CSD and level population of plasma ions

EEDF of warm plasma electrons

Precise measurement of space-resolved electron and ion properties

[4] D. Mascali, A. Musumarra, F. Leone, F.P. Romano, A. Galatá, S. Gammino and C. Massimi, Eur. Phys. J. A **53**, 145 (2017).
[8] K. Takahashi and K. Yokoi, Nucl. Phys. A (1963)

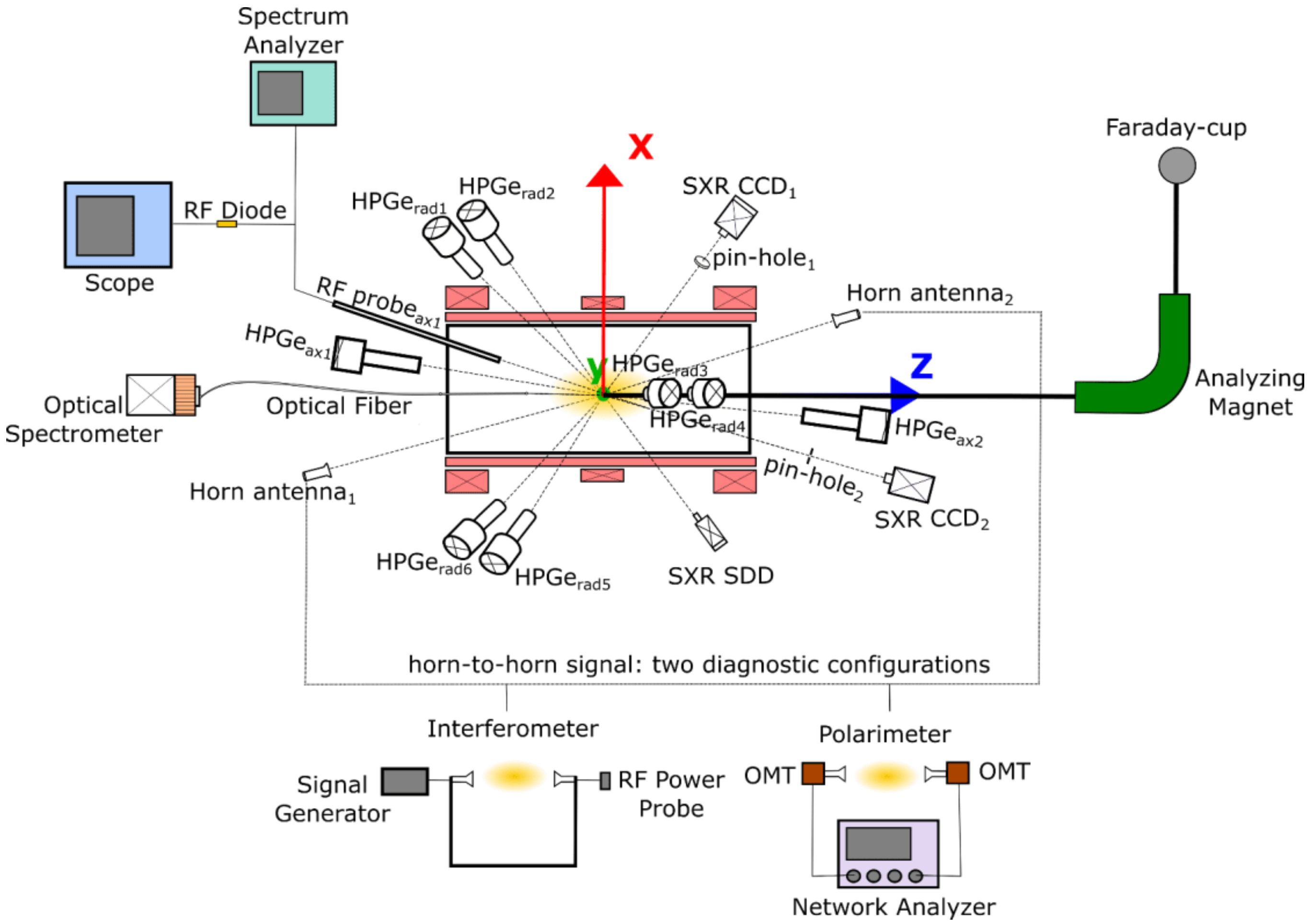

Multidiagnostic setup at LNS [4]

[4] D. Mascali, A. Musumarra, F. Leone, F.P. Romano, A. Galatá, S. Gammino and C. Massimi, Eur. Phys. J. A **53**, 145 (2017).
[8] K. Takahashi and K. Yokoi, Nucl. Phys. A (1963)

Emission spectroscopy excellent indirect diagnostic tool

Different energy ranges of electrons can be probed by analysing different photon ranges

- **Optical spectra for T_e ~ 10 eV [9]**
- **Fluorescence and low energy bremsstrahlung for T_e ~ 10 keV**
- **ECE and bremsstrahlung for T_e > 50 keV [10]**

Novel plasma diagnostic technique developed by ATOMKI, Debrecen and LNS, Catania [6,11,12] – overall objective to study ECR plasma properties through multiple perspectives: space-resolved X-ray images, volumetric X-ray emission and ion current extraction

For high energy bremsstrahlung and contribution from extraction plate

For measuring ion currents (total and individual charge states)

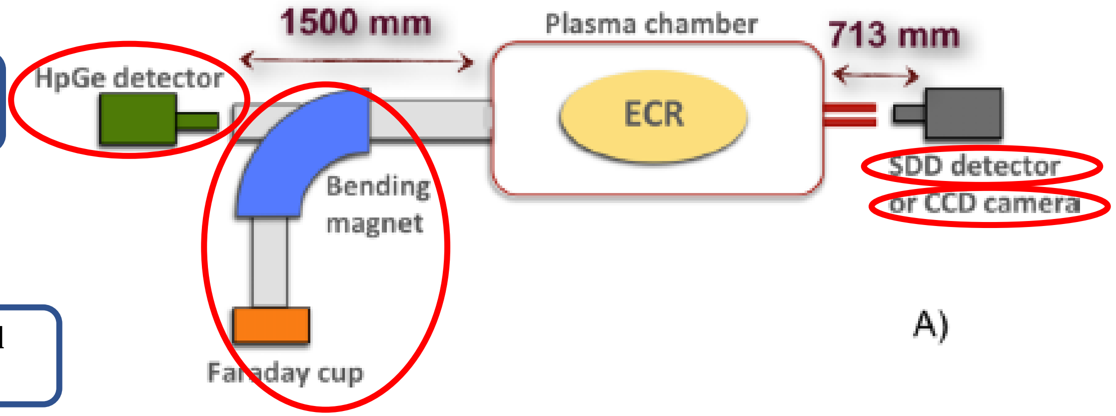

For volumetric fluorescence and low energy bremsstrahlung emission

For 2D space-resolved X-ray imaging (spectrally integrated and photon counting mode)

Schematic of experimental setup showing various detectors used and distances [11]

[6] R. Racz, D. Mascali, S. Biri, C. Caliri, G. Castro, A. Galata, S. Gammino, L. Neri, J. Palinkas, F.P. Romano and G. Torrisi, Plasma Sources Sci. Technol. **26**, 075011 (2017).
[11] D. Mascali, G. Castro, S. Biri, R. Racz, J. Palinkas, C. Caliri, L. Celona, L. Neri, F. P. Romano, G, Torrisi and S. Gammino, Rev. Sci. Instrum. **87**, 02A510 (2016).
[12] R. Racz, S. Biri, J. Palinkas, D. Mascali, G. Castro, C. Caliri, F.P. Romano and S. Gammino, Rev. Sci. Instrum. **87**, 02A741 (2016).

2D Space-Resolved X-Ray Imaging – Experiment Details

Soft X-ray pin-hole camera tool

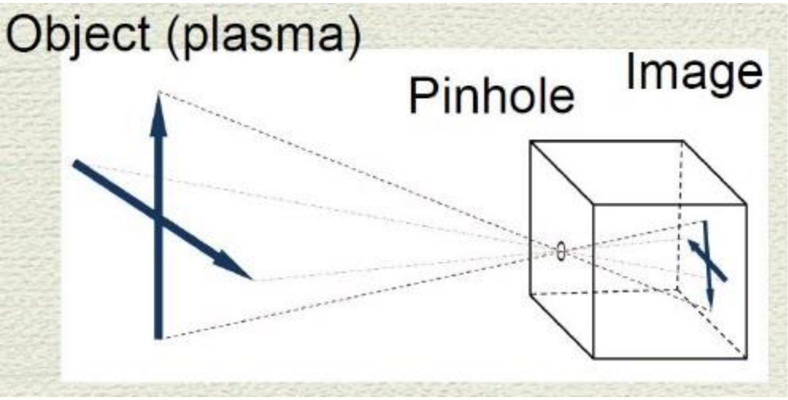

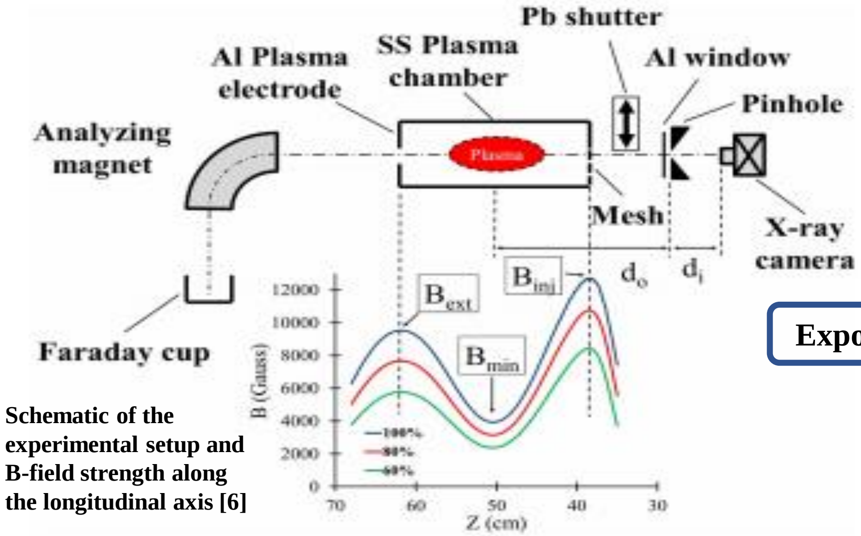

Schematic of the experimental setup and B-field strength along the longitudinal axis [6]

- **Sensitivity range ~ 2 ÷ 15 keV**
- Sensor Size: 27.6 mm x 6.9 mm (1024 x 255 Pixels)
- Pixel size: 13 µm x 13 µm
- Max Energy Resolution ~ 150 eV
- Lead Pin-hole (diameters 100 µm)

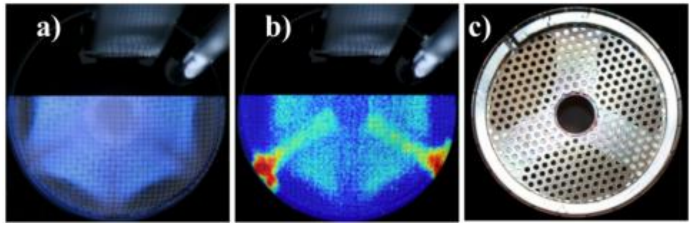

View of the plasma as seen (a) in the optical range, (b) X-ray range and (c) plasma electrode [11]

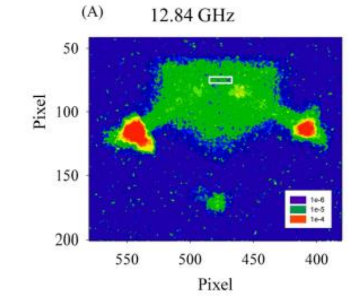

Spectrally integrated plasma images [6]

Exposure modes

Spectrally Integrated:
Long exposure time (in tens of seconds)
Loss of info on individual photon energy
For study of shape, structure and local energy content of plasma

Spectrally Resolved (Photon Counting):
Multiple frames with short exposure time (in ms)
Spatial and spectral resolution possible
Local electron energy distribution and fine structure of plasma studied

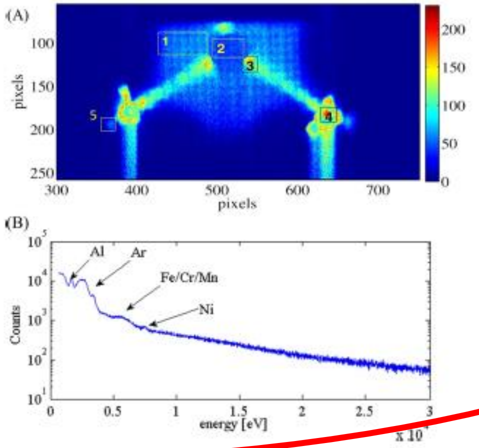

Superposed photon counted frames (A) and corresponding full spectrum (B) for 30 W Ar plasma [6]

[6] R. Racz, D. Mascali, S. Biri, C. Caliri, G. Castro, A. Galata, S. Gammino, L. Neri, J. Palinkas, F.P. Romano and G. Torrisi, Plasma Sources Sci. Technol. **26**, 075011 (2017).
[11] D. Mascali, G. Castro, S. Biri, R. Racz, J. Palinkas, C. Caliri, L. Celona, L. Neri, F. P. Romano, G, Torrisi and S. Gammino, Rev. Sci. Instrum. **87**, 02A510 (2016).

2D Space-Resolved X-Ray Imaging – Theoretical Model: General Outline

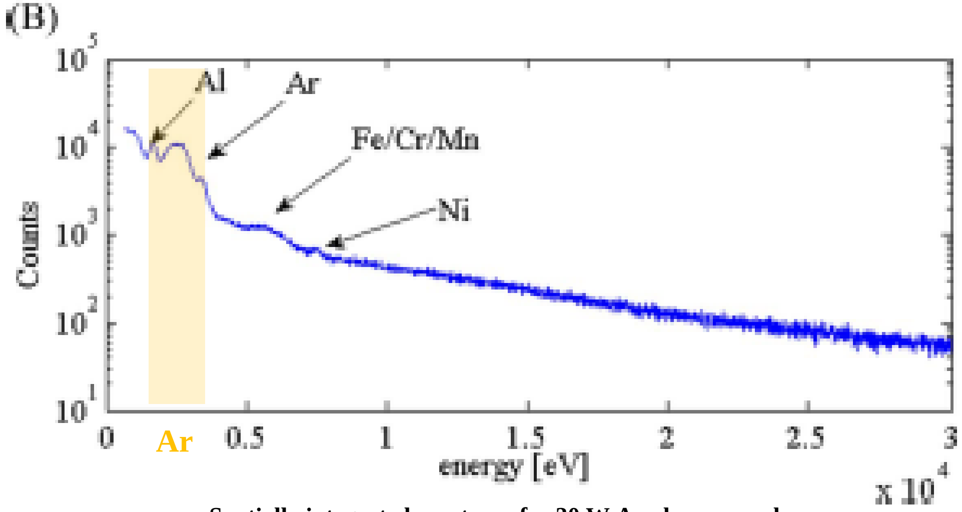

Spatially integrated spectrum for 30 W Ar plasma , and spectral filtering for Ar Kα fluorescence[6]

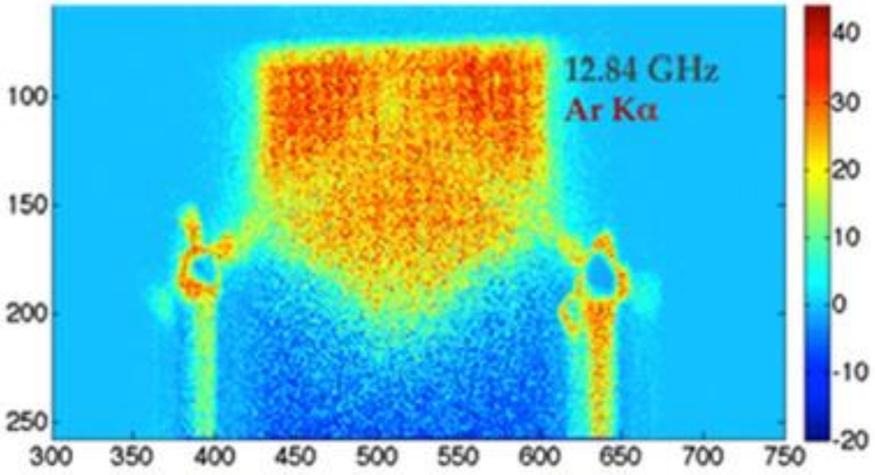

2D space-resolved X-ray map after spectral filtering at 2.96 keV [6]

Kα emission rate

$$R = \rho_e \rho_i \omega_{K\alpha} \int_{3.205}^{\infty} \sigma_{K,ion}(E) v_e(E) f(E) \mathrm{d}E$$

Photon counting mode, 2000 frames taken, exposure time = 150 ms/frame.

$$T = 300 \rho_e \rho_i \omega_{K\alpha} \int_{3.205}^{\infty} \sigma_{K,ion}(E) v_e(E) f(E) \mathrm{d}E$$

Anisotropic and non-homogenous emission source, space-resolved geometrical efficiency

$$T = 300 \boxed{\rho_e \rho_i} \omega_{K\alpha} \boxed{\varepsilon_g} \varepsilon_q \int_{3.205}^{\infty} \boxed{\sigma_{K,ion}(E)} v_e(E) \boxed{f(E)} \mathrm{d}E$$

Local geometrical efficiency

K-shell ionisation cross-section

3D space-resolved electron and ion density and EEDF

[6] R. Racz, D. Mascali, S. Biri, C. Caliri, G. Castro, A. Galata, S. Gammino, L. Neri, J. Palinkas, F.P. Romano and G. Torrisi, Plasma Sources Sci. Technol. **26**, 075011 (2017).

2D Space-Resolved X-Ray Imaging – Theoretical Model: Electron Kinetics

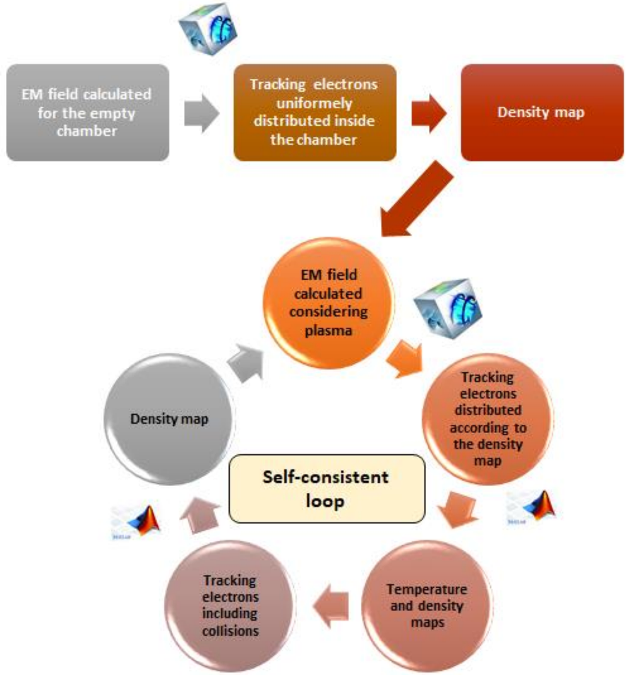

Schematic of COMSOL Multiphysics© + MATLAB© self-consistent numerical modelling for electrons [13]

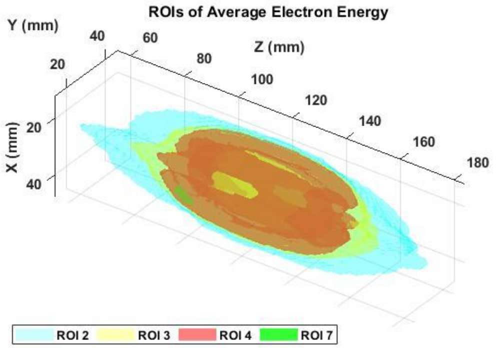

Isosurfaces of constant AVE

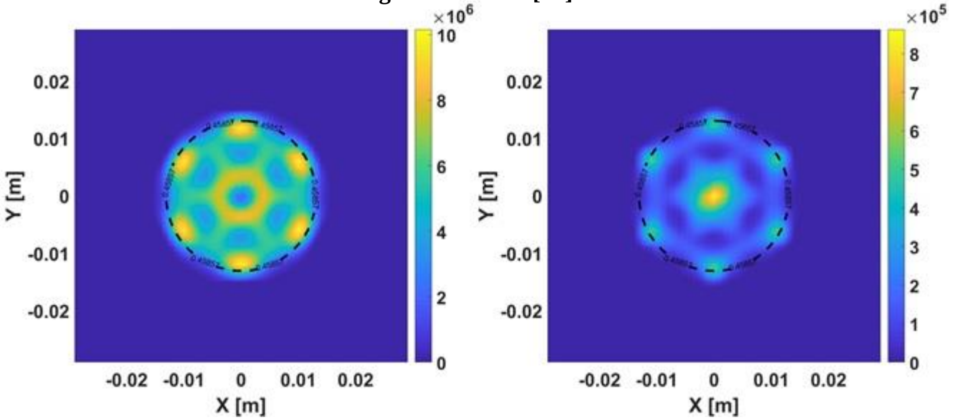

XY-projections of occupation maps in [2,4] keV (left) and [6,8] keV (right)

4 choices of EEDF – mix of Maxwell and Druyvesteyn distribution functions

Ref. case name	Type
EEDF1	Low-E f_M + High-E f_M
EEDF2	Low-E f_M + High-E f_D
EEDF3	Low-E f_M + Medium-E f_M + High-E f_M
EEDF4	Low-E f_M + Medium-E f_D + High-E f_M

$$f_M(E;k_BT_e) = \frac{2}{\sqrt{\pi}}\frac{\sqrt{E}}{(\sqrt{k_BT_e})^3}e^{-E/k_BT_e}$$

$$f_D(E;k_BT_e) = 1.04\frac{\sqrt{E}}{(\sqrt{k_BT_e})^3}e^{-0.55E^2/(k_BT_e)^2}.$$

Each EEDF tested in each ROI – better and more physical analysis

MSE and r² calculated for each cell of the ROI, then mean and SD of both quantities evaluated

Mean – average value of the statistic in the ROI

SD – variation of actual value from the mean *within* the ROI

Thus, low mean MSE, high mean r², and low SD for both implies best performance

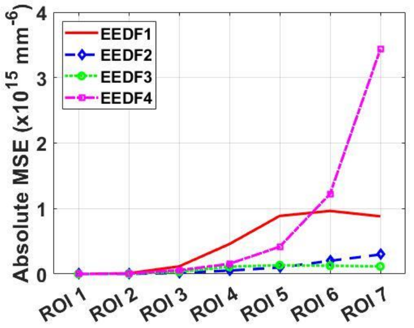

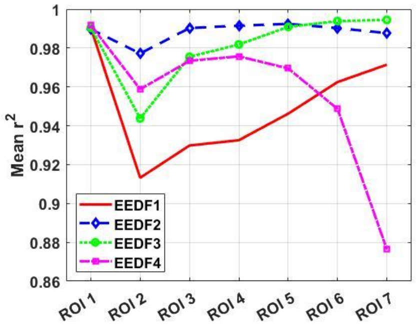

EEDF2 = Cold Maxwell + Hot Druyvesteyn works in each ROI [14]
But simulations give relative electron density distribution, absolute n_e unknown still

[13] A. Galata, C.S. Gallo, D. Mascali and G. Torrisi, eprint arXiv:1912.01988
[14] B. Mishra, accepted to be published, Il Nuovo Cimeno 2021

Lotz formula for K-shell ionisation cross-section

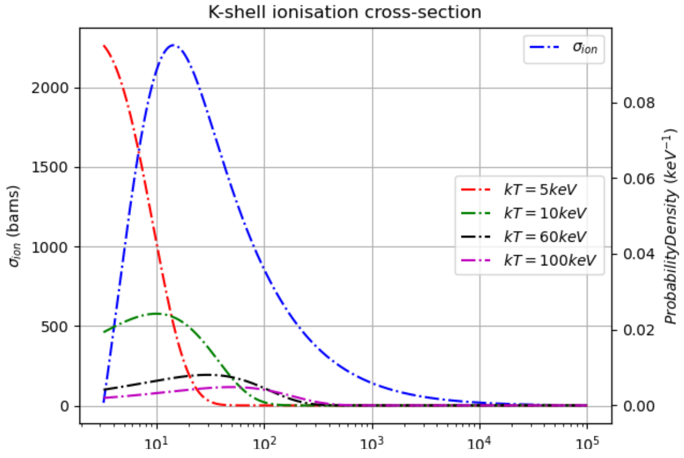

Lotz cross-section for Ar superposed on Maxwell EEDFs at different temperatures [15]

Strong indication that warm electrons 2-30 keV cannot reproduce experimental map with physically valid n_e

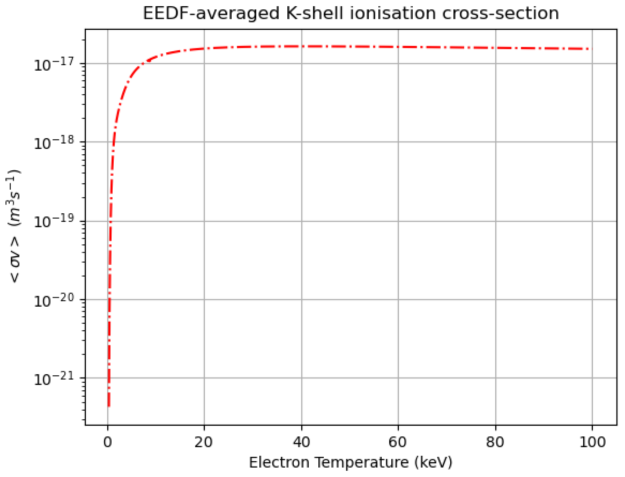

EEDF averaged cross-section for different temperatures [15]

Spatially-resolved geometrical efficiency for anisotropic and non-homogeneous emitting source

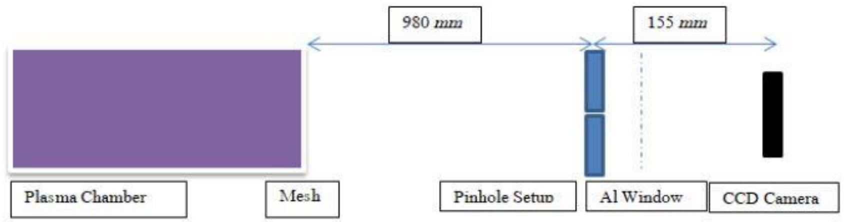

Schematic of the detection system

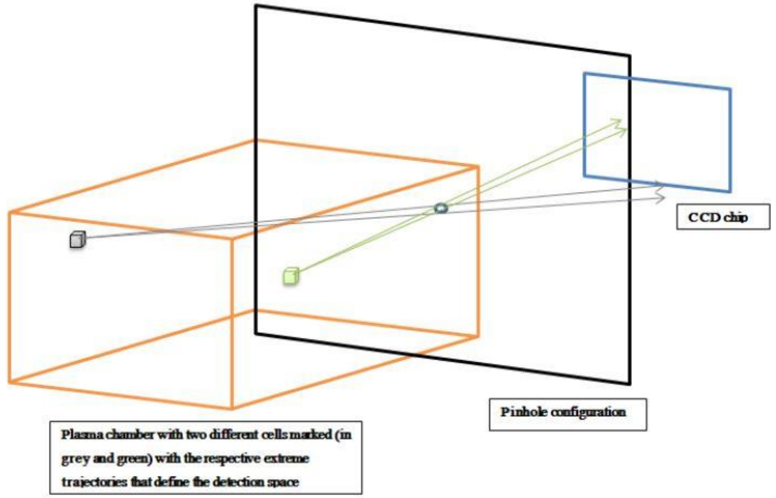

Isometric view of the chamber, pinhole and CCD for ray-tracing

Ray-Tracing Monte Carlo code to evaluate a *3D* map of geometrical efficiency, a value for each plasma cell

[15] B. Mishra, to be submitted to Phys. Of Plasmas

2D Space-Resolved X-Ray Imaging – Theoretical Model: LGE (contd.)

Step 1: Determination of emission space for each plasma cell as defined by pinhole configuration

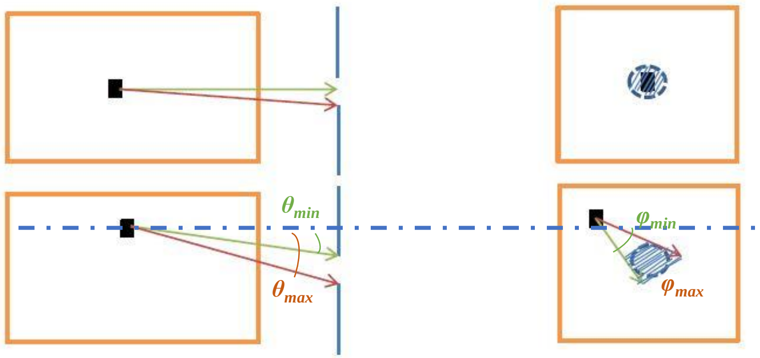

Side and front views of the setup for calculation of position-dependent emission space

$$\Delta\Omega = \int_{\theta_{min}}^{\theta_{max}} \int_{\phi_{min}}^{\phi_{max}} \sin\theta \mathrm{d}\theta \mathrm{d}\phi = (\cos\theta_{min} - \cos\theta_{max})(\phi_{max} - \phi_{min})$$

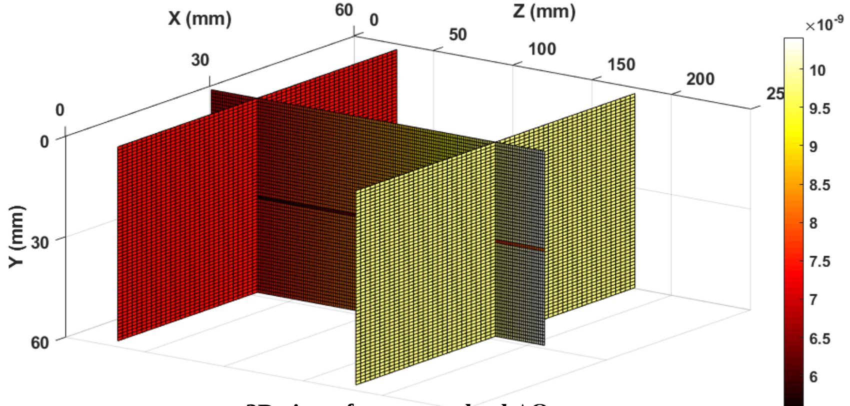

3D view of space-resolved ΔΩ

$$\varepsilon_g = \frac{\Delta\Omega}{4\pi}$$

Step 2: Calculation of photon detection probability through ray-tracing

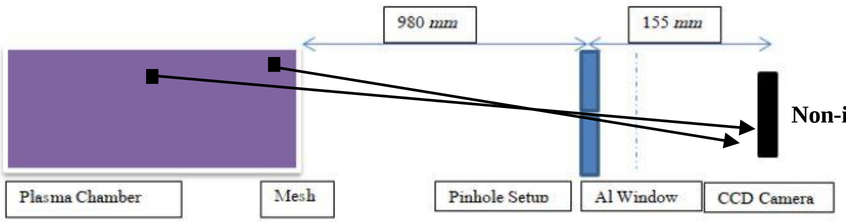

Non-interception by CCD

Transparency 56%

Absorption by window

Corrective factor to bare emission ε_g – simulate N photons within emission space and calculate LGE

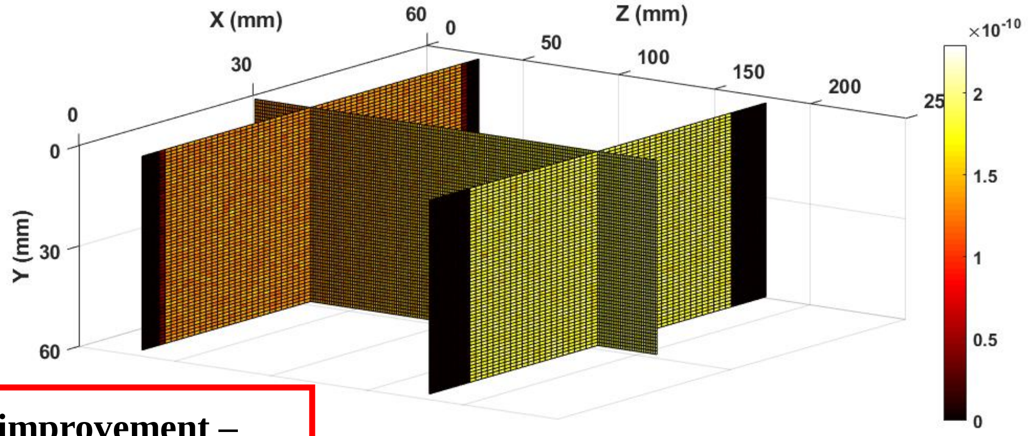

3D view of LGE

LGE calculation still needs improvement – simulation of mesh, scattering effects, plasma self-absorption and contribution from plasma electrode

2D Space-Resolved X-Ray Imaging – Comparison and Conclusion

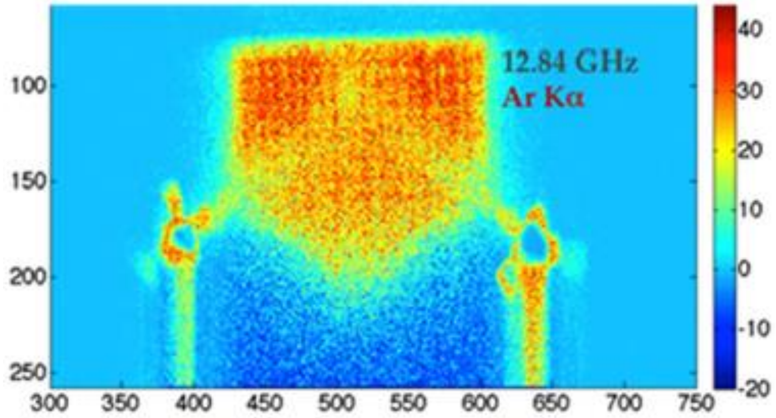

Experimental map - 2D space-resolved X-ray map after spectral filtering at 2.96 keV [6]

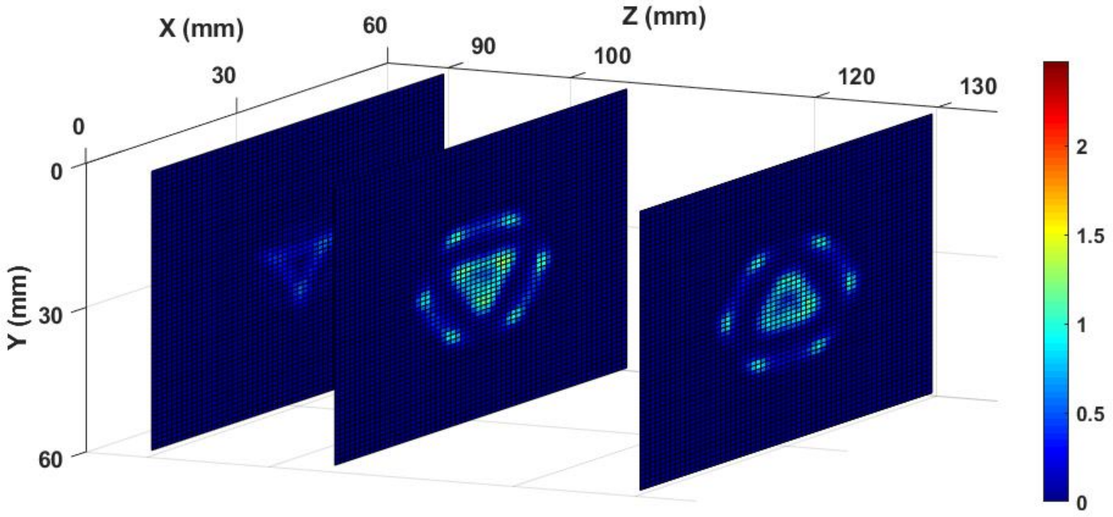

Current calculations have reproduced overall photon counts and structure BUT n_e taken 10^{18} m^3, unphysically high

Direct consequence of considering only electrons between 2-30 keV – very small contribution

Verification needed for n_e from volumetric spectrum analysis

Sliced and longitudinally integrated view of 2.96 keV photon counts

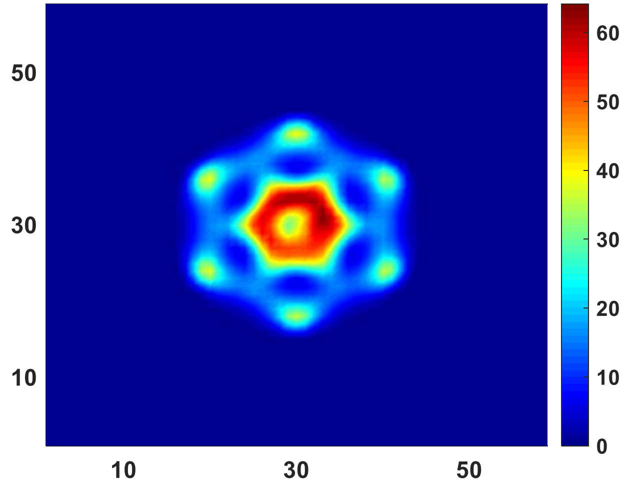

$$T = 300 \rho_e \rho_i \omega_{K\alpha} \varepsilon_g \varepsilon_q \int_{3.205}^{\infty} \sigma_{K,ion}(E) v_e(E) f(E) \mathrm{d}E$$

[6] R. Racz, D. Mascali, S. Biri, C. Caliri, G. Castro, A. Galata, S. Gammino, L. Neri, J. Palinkas, F.P. Romano and G. Torrisi, Plasma Sources Sci. Technol. **26**, 075011 (2017).

Volumetric X-Ray Spectroscopy – Experiment Details

Soft X-ray collimator setup

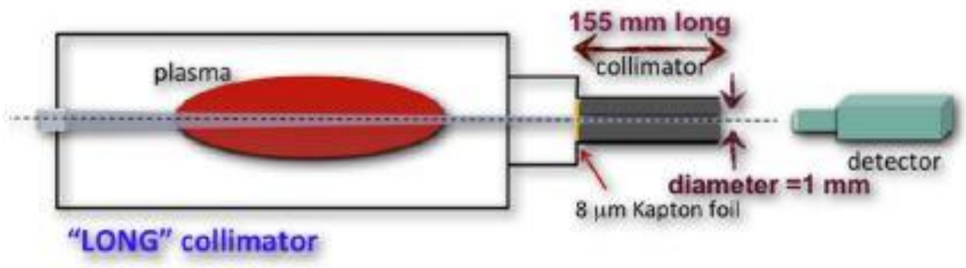

Schematic of the experimental setup showing usefulness of collimator in filtering out emission from the walls/extraction plate [11]

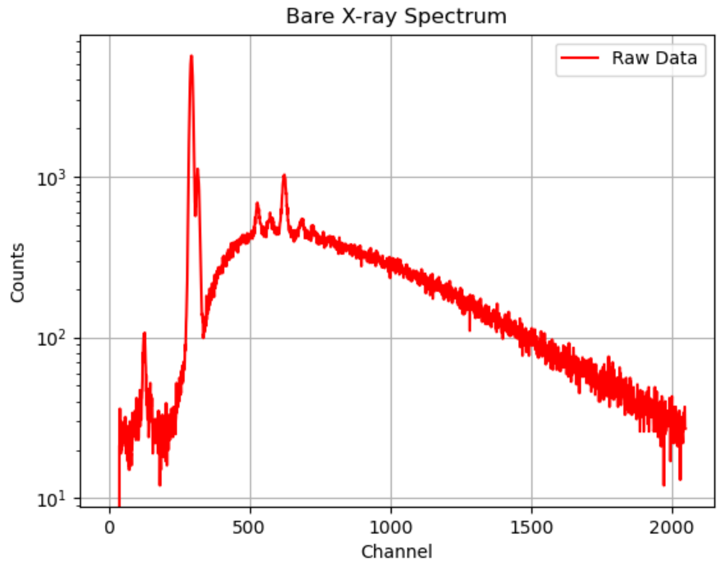

Bare and uncalibrated spectrum from SDD detector

Contribution from bremsstrahlung, Ar fluorescence (confined electrons) and Cr/Fe fluorescence (escaping electrons)

SDD detector used for soft X-ray spectroscopy with energy range 2-30 keV

Long collimator configuration for measuring plasma emission in near-axis region

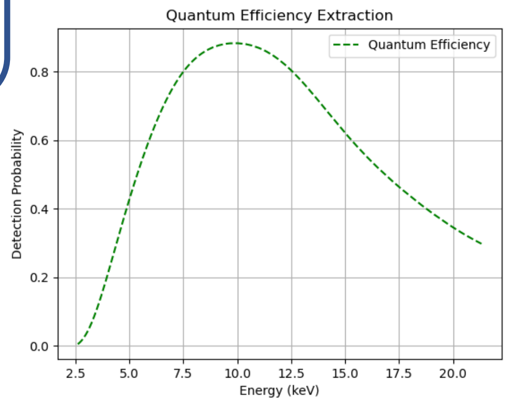

Calibration with Fe lines
+
QE renormalisation
+
Dead time correction+
+
Conversion to emissivity density

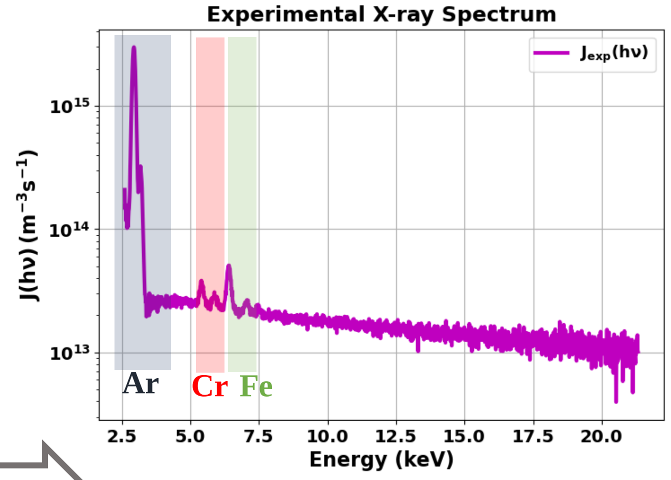

Emissivity density of Ar Plasma [15]

- **Sensitivity range ~ 2 ÷ 30 keV**
- Max Energy Resolution ~ 150 eV
- Collimator length

$$J(h\nu) = h\nu \frac{N^p(h\nu)}{t} \frac{4\pi}{\Delta E V_P \Omega_g}$$

[11] D. Mascali, G. Castro, S. Biri, R. Racz, J. Palinkas, C. Caliri, L. Celona, L. Neri, F. P. Romano, G, Torrisi and S. Gammino, Rev. Sci. Instrum. **87**, 02A510 (2016).
[15] B. Mishra, to be submitted to Phys. Of Plasmas

Volumetric X-Ray Spectroscopy – Theoretical Model: Formalism

Bremsstrahlung Emissivity Density

$$J_{theo,brem}(h\nu) = \rho_e \rho_i \int_{h\nu}^{\infty} \frac{\mathrm{d}\sigma_K(h\nu)}{\mathrm{d}h\nu} v_e(E) f(E) \mathrm{d}E$$

$$\Downarrow$$

Kramer's formula for differential cross-section

$$\frac{\mathrm{d}\sigma_K(h\nu)}{\mathrm{d}h\nu} = \frac{16\pi}{3\sqrt{3}} \alpha^3 \left(\frac{\hbar}{m_e c}\right)^2 \left(\frac{c}{v_e}\right)^2 \frac{Z^2}{h\nu}$$

$$\Downarrow$$

Single-component Maxwell EEDF

$$f_M(E; k_B T_e) = \frac{2}{\sqrt{\pi}} \frac{\sqrt{E}}{(\sqrt{k_B T_e})^3} e^{-E/k_B T_e}$$

$$\Downarrow$$

$$\boxed{J_{theo,brem}(h\nu) = \rho_e \rho_i (Z\hbar)^2 \left(\frac{4\alpha}{\sqrt{6m_e}}\right)^3 \left(\frac{\pi}{k_B T_e}\right)^{1/2} \mathrm{e}^{h\nu/k_B T_e}}$$

Fluorescence Emissivity Density (Ar ions)

$$J_{theo,2.96} = \frac{h\nu_{2.96}}{\Delta E} \rho_e \rho_i \omega_{2.96} \int_{3.205}^{\infty} \sigma_{K,ion}(E) v_e(E) f(E) \mathrm{d}E$$

$$J_{theo,3.19} = \frac{h\nu_{3.19}}{\Delta E} \rho_e \rho_i \omega_{3.19} \int_{3.205}^{\infty} \sigma_{K,ion}(E) v_e(E) f(E) \mathrm{d}E$$

$$\Downarrow$$

Lotz formula for K-shell ionisation cross-section

$$\sigma_{K,ion} = a_K q_K \frac{\ln \varepsilon / I}{\varepsilon I} \{1 - b_K \exp[-c_K(\varepsilon/I - 1)]\}$$

$$\Downarrow$$

Pseudo-Voigt profile for line-broadening

$$D_{PV}(x - x_0, f) = \eta L(x - x_0, \tau_L) + (1 - \eta) G(x - x_0, \sigma_G)$$

$$\Downarrow$$

$$\boxed{\begin{aligned} J_{theo,line,plasma}(h\nu) = [&J_{theo,2.96} D_{PV}(h\nu - 2.96, f_{2.96}) + \\ &J_{theo,3.19} D_{PV}(h\nu - 3.19, f_{3.19})] \Delta E \end{aligned}}$$

Fluorescence Emissivity Density (Cr/Fe atoms)

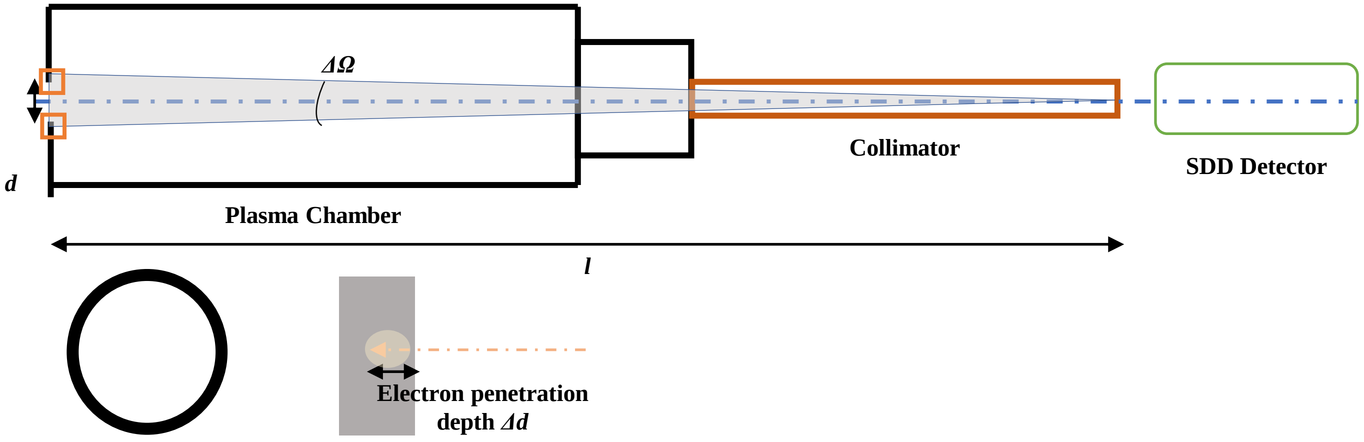

Active emission area = $4\pi\varepsilon_{gl}^2 - \pi d^2/4$

$$J_{theo,h\nu} = \frac{h\nu}{V_P \Delta E} \rho_{e,loss} N_t \int_I^\infty \sigma_{K,ion}(E) v_e(E) f(E) \mathrm{d}E$$

Deutsch-Mark formalism for K-shell ionisation cross-section

$$\sigma_{1s,ion} = g_{1s}\pi(r_{1s})^2 \xi_{1s} f(U) F(U)$$

Estimation of number of target atoms N_t

$$N_t(E) = n_t\left(4\pi\varepsilon_g l^2 - \pi\frac{d^2}{4}\right)\Delta d(E)$$

Parametrisation of penetration depth as a function of energy

$$J_{theo,h\nu} = \frac{h\nu}{V_P \Delta E} \rho_{e,loss} n_t \left(4\pi\varepsilon_g l^2 - \pi\frac{d^2}{4}\right) \int_I^\infty v_e(E) f(E) \int_E^I \frac{1}{S(E)} \sigma_{K,ion}(E') \mathrm{d}E' \mathrm{d}E$$

Pseudo-Voigt profile for line-broadening

$$\boxed{J_{theo,line,loss}(h\nu) = \sum J_{theo,h\nu_0} D_{PV}(h\nu - h\nu_0, f_{h\nu_0}) \Delta E}$$

Volumetric X-Ray Spectroscopy – Theoretical Model: Cross-Section

Fluorescence from plasma interior – Ar ions and confined electrons

Lotz formula for K-shell ionisation cross-section

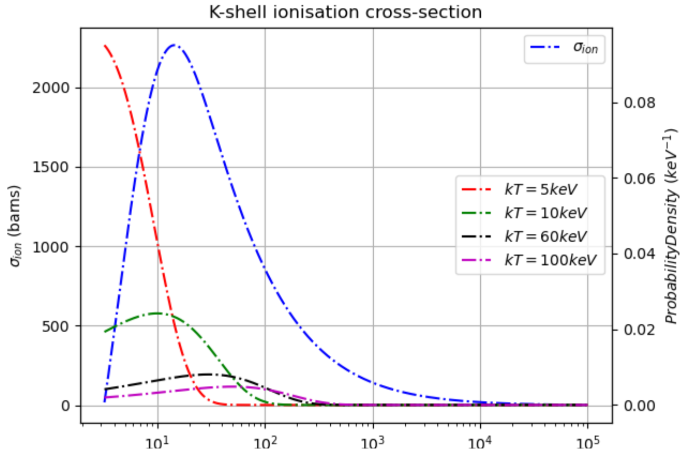

Lotz cross-section for Ar superposed on Maxwell EEDFs at different temperatures [15]

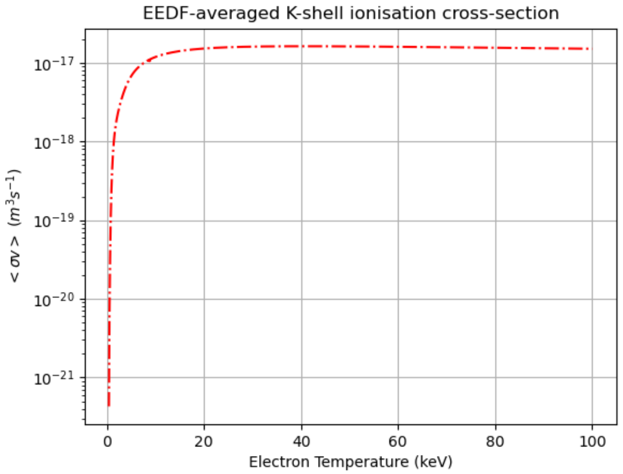

EEDF averaged cross-section for different temperatures [15]

Ineffective overlap for low temperatures, major contribution from $k_B T_e$ ~ 10 keV

Fluorescence from extraction plate – Cr/Fe atoms and escaping electrons

Deutsch-Mark formalism for K-shell ionisation cross-section

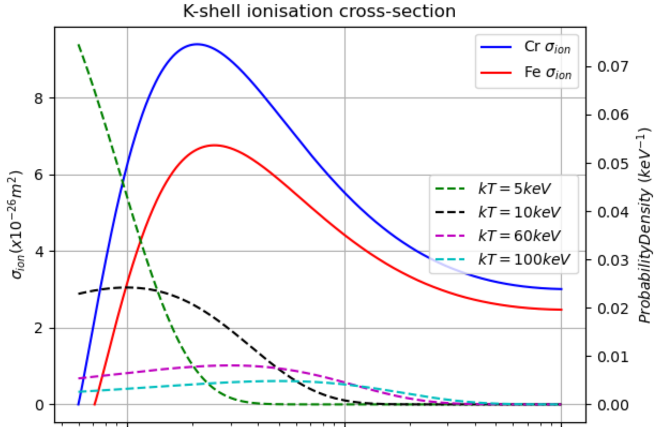

Lotz cross-section for Cr/Fe superposed on Maxwell EEDFs at different temperatures [15]

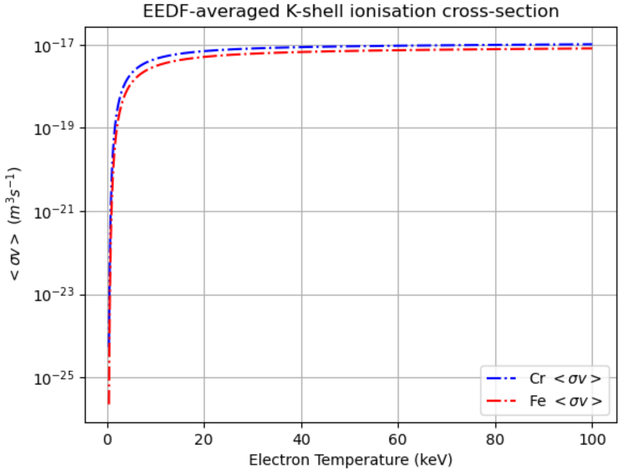

EEDF averaged cross-section for different temperatures [15]

[15] B. Mishra, to be submitted to Phys. Of Plasmas

Volumetric X-Ray Spectroscopy – Comparison and Conclusion

Product of confined plasma electron and ion density $\rho_e \rho_i$ obtained ~ 1.32x10^32 m^{-3}, expected n_e ~ 10^{16} m^{-3}

EEDF is single Maxwellian – T_e ~ 21.15 keV

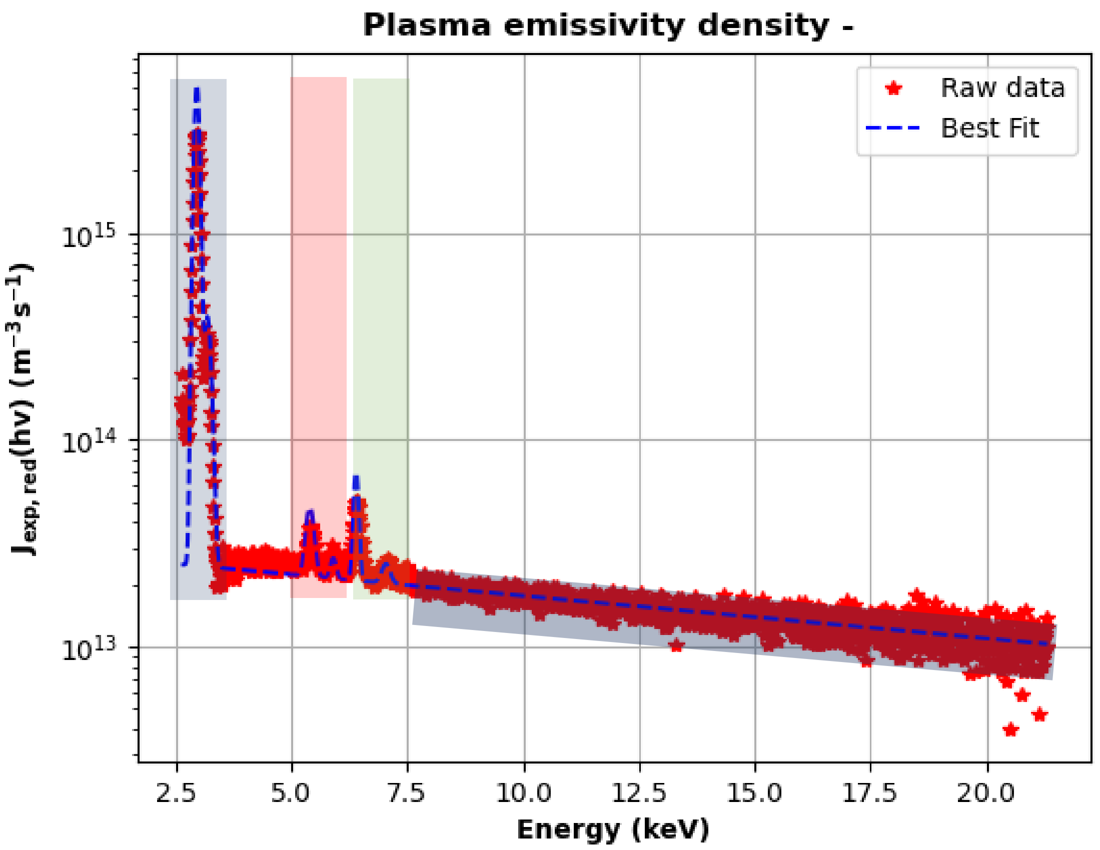

Escaping electron density $\rho_{e,loss}$ ~ 10^{12} m^{-3}, estimated j_{av} ~ 2-3 mA/cm^2

Matches ion current density to order of magnitude

Chosen model fits experimental data well and gives valuable information about confined and escaping electrons

Conclusions

Space-resolved X-ray Imaging

Theoretical model developed based on self-consistent numerical simulations on warm electrons + LGE evaluation

Preliminary results show match with respect to overall structure (correlated with simulations/relative distribution) and counts (correlated with absolute particle density)

Uncertainties in both experimental and theoretical counts – n_e used too high owing to small contribution from warm electrons, corroborated with volumetric analysis

UPDATE SIMULATIONS

CONSIDER HOTTER ELECTRONS

IMPROVE LGE + OVERALL MODEL

Volumetric X-Ray Spectroscopy

Theoretical model developed based on bremsstrahlung and fluorescence from trapped particles and fluorescence from escaping electrons impinging on extraction plate

Excellent match between model and experiment, fit procedure furnishes particle density in expected range, predicts contribution from hotter electrons towards Kα emissions

Sandor Biri
Richard Rácz

David Mascali
Domenico Santonocito
Angelo Pidatella
Eugenia Naselli
Maria Mazzaglia
Giorgio Mauro
Giuseppe Torrisi

Alessio Galatà

THANK YOU FOR YOUR ATTENTION!